Poly(lactic) acid/carbon nanotube composite microneedle arrays for dermal biosensing

Eldhose Skaria[*1], Bhavik A. Patel[1,2], Melanie S. Flint[1,2], Keng Wooi Ng[*1,3]

[1]School of Pharmacy and Biomolecular Sciences and [2]Centre for Stress and Age-Related Diseases, University of Brighton, Huxley Building, Lewes Road, Brighton, BN2 4GJ, United Kingdom.

[3]School of Pharmacy, Faculty of Medical Sciences, Newcastle University, King George VI Building, Queen Victoria Road, Newcastle upon Tyne, NE1 7RU, United Kingdom.

ABSTRACT: Minimally invasive, reliable and low-cost *in vivo* biosensors that enable real-time detection and monitoring of clinically relevant molecules and biomarkers can significantly improve patient healthcare. Microneedle array (MNA) based electrochemical sensors offer exciting prospects in this respect, as they can sample directly from the skin. However, their acceptability is dependent on developing a highly scalable and cost-effective fabrication strategy. In this work, we evaluated the potential for poly(lactic) acid/carboxyl-multiwalled carbon nanotube (PLA/*f*-MWCNT) composites to be developed into MNA's and their effectiveness for dermal biosensing. Our results show that MNA's are easily made from solvent casted nanocomposite films by micromoulding. A maximum carbon nanotube (CNT) loading of 6 wt% was attained with the current fabrication method. The MNA's were mechanically robust, being able to withstand axial forces up to 4 times higher than necessary for skin insertion. Electrochemical characterisation of these MNA's by differential pulse voltammetry (DPV) produced a linear current response towards ascorbic acid, with a limit of detection of 180 µM. *In situ* electrochemical performance was assessed by DPV measurements in ex vivo porcine skin. This showed active changes characterised by two oxidative peaks at 0.23 and 0.69 V, as a result of the diffusion of phosphate buffered saline. The diagnostic potential of this waveform was further evaluated through a burn wound model. This showed an attenuated oxidative response at 0.69 V. Importantly, the impact of the burn could be measured at progressive distances from the burn site. Overall, alongside the scalable fabrication strategy, the DPV results promise efficient electrochemical biosensors based on CNT nanocomposite MNA's.

Dermal biosensing is an emerging trend in mobile healthcare technologies. Dermal biosensing devices aim to provide cost-effective, decentralised and rapid health monitoring in a non-invasive manner[1]. Broadly, such devices can be classified into skin-worn surface electrodes or needle-like penetrable biosensors. These classes of devices commonly analyse sweat or the interstitial fluid (ISF), respectively, as the source of biological information. Among these, skin-penetrating microneedle array (MNA) biosensors have attracted significant research interest due to their ability to access the dermal ISF without causing pain or bleeding, while gathering a wealth of information concerning disease markers and metabolites. The relative abundance of health markers in the ISF renders excellent analytical sensitivity to MNA biosensors, whilst a guaranteed skin-electrode contact enables high spatial resolution without compromising the signal-to-noise ratio. Since each microneedle on a MNA biosensor can be individually addressed, multiplex detection is possible. Importantly, the electrochemical detection strategies employed are generally low-cost, facile and can be effectively utilised by a minimally trained individual at the point of care[2].

Research to date have demonstrated several approaches towards the fabrication of MNA-based electrodes. One that is commonly employed to design various sensors is a concept introduced by Windmiller and colleagues[3,4]. They showed that, modified carbon fibres and pastes, concealed within a hollow MNA can effectively function as an electrochemical transducer; producing highly selective and sensitive responses for hydrogen peroxide, lactate and ascorbic acid (AA). By adopting this bi-component design, recent studies have successfully developed MNA based enzymatic sensors towards continuous monitoring of alcohol[5] and detection of organophosphorus nerve agents[6]. Miller *et al.* further established this strategy as effective for multiplexing capabilities, by individually addressing each microneedle in an array, to enable simultaneous detection of glucose, lactate and pH[7]. These results have proven this bi-component design to be an attractive platform to develop MNA-based sensors.

In comparison to hollow MNA-based sensors, sensors developed from solid MNA-based electrodes can be advantageous in many aspects, including fabrication, application and analytics. Foremost, solid microneedle-based electrodes have a larger electroactive surface area for biomolecular detection[8]. The overall current response generated is therefore greater, alongside improved sensitivity. In terms of application, solid microneedles can eliminate issues associated with clogging and offer better mechanical robustness[9]. Until recently, solid MNA-based sensors have been fabricated from micromachined or lithographically processed silicon or metallic MNA's, that are then coated with gold or platinum using e-beam lithography or by sputtering (i.e. metallisation) and functionalised with oxidase enzymes for specific detection of analytes[9–12]. Recent progress has simplified this approach significantly by implementing micromoulding as a facile fabrication strategy[13–15]. Whilst initial attempts replaced existing MNA's with polymeric counterparts[13,14], McConville and Davies introduced the use of composite formulations (i.e. palladium (Pd) microparticles embedded in a polymeric matrix) to develop MNA-based electrodes[15]. The

latter is highly attractive because cost-effective and versatile formulations can be produced with desirable functional and mechanical properties using a wide range of materials. However, a major challenge associated with composite formulations is to define an optimal ratio at which conductive fillers are to be incorporated to achieve the desired mechanical and electrochemical properties.

A very high filler ratio (≥50%) is necessary to facilitate excellent bulk conductivities for composites incorporating submicron-sized particulate fillers such as Pd[15]. This not only incurs high manufacturing costs, but also poses significant challenges to processing due to the increased viscosity. Particle aggregation from poor dispersibility and weak interfacial adhesion between the filler and the host matrix can further result in mechanical failure of the microneedles during application. Thus, attaining a sufficiently low filler ratio is crucial; especially to maintain composite processability similar to their polymeric matrices. This will be highly advantageous, as MNA-based electrodes may then be rapidly prototyped in a single-step using a scalable fabrication method, e.g. through composite film synthesis and injection moulding.

In comparison to the various conductive fillers, carbon nanotubes (CNT's) are better suited as active materials within polymeric matrices to form multifunctional nanocomposites. CNT's are distinguished by their unique tubular nanostructure, with a larger aspect ratio and ultra-high specific surface area, alongside excellent mechanical, electrical and electrocatalytic properties. Critically, improvements in electrical conductivity for well-dispersed CNT-based nanocomposites have been reported at extremely low percolation thresholds, i.e. <1 wt%, which also acts to improve mechanical properties[16]. Electrochemical sensing based on CNT's is an established field, but they have been used primarily as modifiers of glassy carbon or gold electrode surfaces[17]. CNT-based nanocomposites can also be developed as electrodes themselves, as indicated by CNT-paste electrodes, where a low-molecular-weight thermosetting resin such as epoxy is typically used as a binder[18–20]. However, the loading ratios of CNT's used to prepare these electrodes remain high, i.e. >15 wt%, limiting the electrode designs to certain sizes and geometries. Nanocomposite manufacturing processes such as solution mixing have been shown to be highly effective in reducing the loading ratios required whilst maximising their physical properties. However, such research has not yet been correlated to electrochemical properties.

In this work, we investigate if MNA's can be fabricated by micromoulding nanocomposite film of poly(lactic) acid (PLA) and carboxyl-functionalised multiwalled carbon nanotubes (f-MWCNT). PLA was chosen due to its excellent mechanical properties for penetrating the skin as MNA's[21], biocompatibility and processability towards the fabrication of nanocomposite films by a solution processing approach [22]. Here, the structural and mechanical properties of the nanocomposite microneedles were assessed to determine their suitability as a penetrable dermal biosensor. Although similar nanocomposites have been used previously for biosensing, it is for the first time PLA/f-MWCNT composites electrodes are being directly connected to an electrochemical analyser for bioanalysis in a MNA format. Analytical performance of the MNA's was assessed in vitro using AA. AA was chosen for its known electrochemical profile and physiological significance, such as its involvement in a number of biochemical pathways and neuromodulatory processes[23]. We also demonstrate *in situ* biosensing capabilities of the MNA's by monitoring dynamic changes in the skin induced by the diffusion of phosphate buffered saline (PBS) in artificial burn wounds.

MATERIALS AND METHODS

MWCNT grown by catalytical chemical vapour deposition and functionalised with carboxyl groups were purchased from Cheap Tubes Inc. (Cambridgeport, USA), with the following specifications—length: 10–30 µm, outer diameter: 20–30 nm, 1.2% functional groups and purity >95 wt%. Poly(lactic) acid filaments was a product of MakerBot Industries, Brooklyn, USA. Polycaprolactone (Polymorph®) was acquired from Mindsets ltd, Essex, UK. Sylgard® 184 silicone elastomer was from Dow Corning (Midland, MI, USA). Ascorbic acid (AA) and methylene blue was purchased from Sigma-Aldrich (Gillingham, UK). Chloroform and agarose were purchased from Fisher Scientific (Loughborough, UK). Electrical wire and steel rods were from RS components Ltd (Corby, Northants, UK). Freshly excised ears were recovered from pigs that had been euthanised for unrelated studies at the Pirbright Institute (Pirbright, UK) and reused in accordance with the 3Rs (replacement, reduction and refinement) principles and ARRIVE guidelines. The porcine ears were transported on ice to the laboratory and used within 3 hours of excision.

Fabrication of PLA/*f*-MWCNT composites. Due to the ease of processing, solution mixing followed by solvent evaporation (i.e. solvent casting) is commonly employed to form CNT based polymeric nanocomposites. In this approach, CNT's are dispersed using a solvent of choice that will then dissolve the polymer of choice. As dispersion is a major challenge due to strong van der Waals interactions between the tubes, a combinatorial approach involving *f*-MWCNT and sonication, in an organic solvent (chloroform), was employed to produce nanocomposites with minimal aggregation. Briefly, *f*-MWCNT at different loadings (3–6 wt% relative to the weight of PLA) was dispersed in chloroform (48 mL) using an ultrasonic bath at 37 kHz for 1 hour. PLA was then dissolved into the dispersed solution by magnetic stirring at 45°C for 1.5 hours. For efficient intercalation with the polymer, the solution was further sonicated for an hour, with the temperature controlled at ~45°C (using the thermostat of the bath sonicator). Final homogenisation was completed by magnetically stirring the solution at 45°C for 48 hours. To obtain a composite film, the mixture was poured into a glass petri dish for solvent evaporation at room temperature for 48 hours. Residual chloroform was removed by drying the film at 60°C overnight in a thermal oven.

Micromoulding. Nanocomposite MNA's were produced by adapting a micromoulding approach originally developed by McAllister et al[24] and previously optimised for producing PLA MNA's in our laboratory[21]. Initially, a micromould (negative template) was produced from the Sylgard®184 elastomer kit against a commercial template MNA (Derma Stamp, amazon.co.uk, ASIN: B007ATO20I). The composite film was then cut into small ~1 × 1 cm pieces and filled into the micromoulds at a specified weight of 0.175 g. The micromoulds were then heated in a thermal oven at 200°C for 2 hours. This caused the composite material inside the micromould to become pliable, upon which it was manually compressed into the microcavities to form the microneedles. This process was repeated three times to ensure MNA formation in the mould. A coiled wire, covering

~85% of the nanocomposite surface, was then affixed by minimal compression while the material was pliable. After a period of cooling to ensure a firm connection with the composite material, the electrical contact was sealed with polycaprolactone by melting it at 100°C over the surface, forming an insulating layer. On further cooling, the MNA was ejected from the mould manually. PLA MNA's were made similarly, but with vacuum assisted micromoulding at 180°C.

Mechanical characterisation. A TA.TX Plus texture analyser (Stable Microsystems Ltd, Surrey, UK) was used to assess microneedle axial failure strength (AFS) and shear failure strength (SFS). To measure AFS, a single microneedle was affixed parallel to the TA measuring probe. Measurement was triggered as the probe sensed a resistance of 0.01 N. Recordings were taken at 0.1 mm s^{-1} until a target force of 5 N was reached. For SFS, individual microneedles were removed manually from the supporting base so that only a single row of microneedles remained to allow for probe clearance whilst testing. The MNA was affixed perpendicular to the TA measuring probe. The probe was aligned to cover ~50% of the microneedle length from the needle tip. Here, the target force was 2 N. Comparisons were made between the nanocomposite and PLA MNA's containing no *f*-MWCNTs.

Electrochemical characterisation. Electrochemical performance of the nanocomposite MNA's was characterised using AA; carried out using a potentiostat (630B, CH Instruments, Austin, TX) with a three-electrode system consisting of an Ag|AgCl (3 M KCl) reference electrode, a platinum wire auxiliary electrode and the MNA's as the working electrodes. Before the test, each MNA was pierced through a layer of Parafilm M® and sealed around the composite by application of heat (40°C for 5 minutes) to ensure responses were from the microneedles alone and not the supporting base. Differential pulse voltammetry (DPV) was used to analyse different concentrations of AA in 0.1 M PBS across a potential window of 0–1 V, using a pulse amplitude of 0.05 V and a pulse width of 60 ms. Response size was quantified as the area under the curve (AUC) to account for peak broadening.

***In situ* analysis.** DPV measurements were made in the skin to evaluate MNA performance as a penetrable biosensor. Full-thickness skin was prepared from fresh pig ears as described previously[25]. One end of the skin was pinched and clamped between the donor and receptor chambers of a Franz diffusion cell. The clamped skin was then pierced with a hypodermic needle to equalise the pressure and allow direct fluid flow between the two chambers. Both chambers were then filled with PBS. The reference and the auxiliary electrodes were placed inside the donor chamber, while the MNA was used to penetrate the skin which in turn securely held the MNA in place for the duration of the experiment. Measurements were taken at regular intervals over 160 minutes using DPV as detailed previously. Control measurements were taken without the diffusion cell set-up. Non-skin control measurements were also made using a 2 cm thick 1% w/v agarose gel (prepared in 0.1 M PBS). Ear skin samples from five animals were used to account for inter-sample variability.

Evaluation in a burn wound model. Once the PBS had diffused into the skin for 160 minutes, controlled burn wounds were induced to the skin using the flat end of stainless-steel rod (12 mm in diameter) heated to 100°C (in a thermal oven) and kept in contact with the skin for 2 minutes. After the burn was induced, PBS was allowed to diffuse into the skin for another 160 minutes. DPV measurements were taken before and after the burn on the same site and on adjacent control (non-burn) sites. To evaluate the diagnostic potential of the electrochemical signature of the skin, the influence of the burn was measured at specified distances from the edge of a burn site. Using the MNA's, DPV responses were measured again at the site of the burn, 1 mm away and 10 mm away. These measurements were taken after allowing PBS diffusion into the skin as before. Responses were measured from five ear skin samples.

Imaging. Microneedle topology and dimensions were analysed using field emission gun scanning electron microscopy (FEG-SEM; Carl Zeiss SIGMA, Germany) after sputter coating the MNA's with a 4 nm layer of gold. MNA perforations in the skin was visualised by methylene blue staining and acquired using a stereo digital microscope equipped with a 3-megapixel camera (SMZ-168, Motic, HK). Photographs of MNA's were taken using a digital camera.

Statistical analysis. Mechanical forces were measured and recorded using the Exponent Lite software (version 6.1.9.0; Stable Microsystems Ltd, Surrey, UK). Similarly, CHI760 (version 14.02; CH Instruments, Inc, Austin, TX, USA) was used to measure DPV traces, with respect to their peak potential and total peak area. GraphPad Prism 7 (GraphPad Software, La Jolla, CA, USA) was used to analyse the data. Where appropriate, statistical differences between groups were assessed using two-sided Student's t-test, repeated measures, one- or two-way analysis of variance (ANOVA). Differences were considered statistically significant where $p < 0.05$. Data are expressed as mean ± standard deviation.

RESULTS AND DISCUSSION

MNA fabrication and physical characterisation. MNA's containing 3–6 wt% of *f*-MWCNT were successfully manufactured; with 6 wt% being the maximum loading amenable with the current fabrication method. Figure 1A–C shows SEM images of a representative composite MNA at 6 wt% *f*-MWCNT loading. Each MNA consisted of 35 microneedles, arranged in 5 rows with a centre-to-centre distance of 1 mm (within rows) and 1.2 mm (between rows). Each microneedle was conical with a slightly convex surface and measured approximately 870 µm in length and 250 µm in base diameter. The slightly rounded tips were approximately 40 µm in diameter (Figure 1B–C). By precisely controlling for the amount of PLA/*f*-MWCNT used in the fabrication process, a consistent microneedle supporting base thickness of ~2 mm was achieved (Figure 1F). This was important in reducing electrochemical variation between the MNA's. Manual compression of the composite during micromoulding produced microneedles with relatively smooth surfaces (Figure 1B, C). However, on inspecting the cross section of a single microneedle (i.e. the stump of a broken microneedle), clusters of CNT's were found alongside dispersed CNT's within the polymeric matrix (Figure 1D, E). The formation of clusters can be attributed to localised aggregation of CNT's during the solvent evaporation process[26,27], which in turn may give rise to CNT-free regions depending on the loading[27]. These characteristics may have a significant impact on the electrical and mechanical properties of the composites. Electrical response from a clustered network has been shown to have a lower percolation threshold than a homogenous network[28,29]. In relation to solvent casting, albeit being inhomogeneous, there

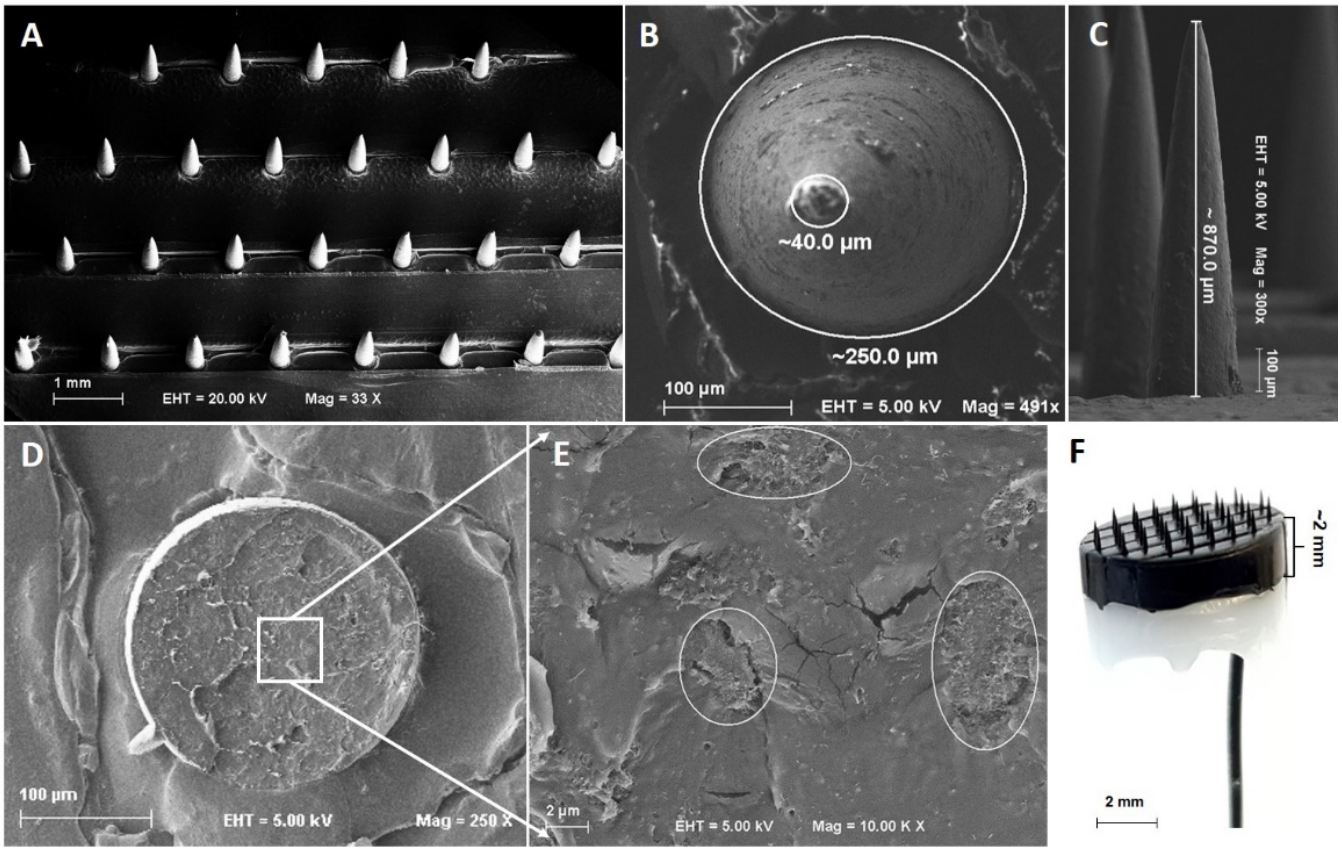

Figure 1. Images of 6 wt% PLA/*f*-MWCNT composite MNA: (A–E, SEM images)—(A) conical microneedles formed consistently by micromoulding. (B) Tip diameter ≈ 40 µm and base diameter ≈ 250 µm. (C) Accessible microneedle height of ≈ 870 µm produced from a 1 mm-long template, with the remaining left inaccessible in between the ridges. (D) Cross-sectional view of a broken microneedle (stump shown). (E) enlarged segment showing aggregates in circles. (F) Photograph of a complete nanocomposite MNA with a composite base height of approximately 2 mm.

is a strong localised interaction between the CNT's and therefore the effective volume fraction of CNT is higher compared to that of a homogenous network[27]. The high CNT loading used here typically produces a vastly agglomerated network. However, this can improve contact between the CNT's once the percolating network has been formed. Moreover, the compressive force applied here would have imparted a certain degree of mobility to the CNT's, thus further improving conductivity by enhancing interactions and contact between the CNT's[27,30,31]. In contrast, it is generally accepted that agglomerates can act as concentrators of physical stress, i.e. they prevent effective load transfer between the polymer and CNT's, rendering the composite more susceptible to mechanical failure[32]. This may not always be the case, however, as a mixture of agglomerates of different sizes could produce tighter CNT packing within the polymer, resulting in a stronger CNT network with better mechanical properties[33].

Mechanical characterisation. The mechanical strength of PLA/*f*-MWCNT MNA's containing 3–6 wt% CNT were evaluated. The percentage of CNT loading can significantly influence the mechanical and electrical properties of polymer-CNT composites. Ultimately, there is a critical value for filler content, below which reinforcement occurs and above which severe deterioration occurs[34], leaving the composite inferior to the matrix alone. Moreover, the composite matrix is non-homogenous as shown previously in the SEM micrographs. Therefore, we anticipated the mechanical properties to vary between the loadings up to 6 wt% and within the MNA's. Hence, individual microneedles were evaluated.

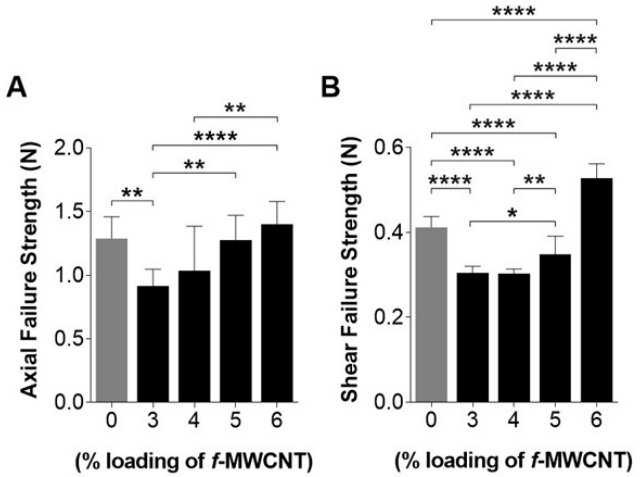

Figure 2. (A) AFS of nanocomposite microneedles increased with increasing loading of *f*-MWCNT. AFS of microneedles with 4–6 wt% *f*-MWCNT loading was comparable to that of neat PLA, whereas 3 wt% was significantly weaker. (B) SFS of nanocomposite microneedles was significantly lower at 3–5 wt% *f*-MWCNT loading. However, at 6 wt% *f*-MWCNT loading, the microneedles yielded a significantly higher SFS compared to that of neat PLA. (*$p < 0.05$, **$p < 0.01$, ***$p < 0.001$, ****$p < 0.0001$, one-way ANOVA with Tukey's multiple comparisons test ($n = 10$).

Figure 2 shows the AFS and SFS of composite MNA's in comparison to PLA MNA's (i.e. 0 wt% CNT). Overall, the microneedles increased in mechanical strength with increasing CNT loading between 3–6 wt%. In relation to AFS (Figure 2A), composite microneedles of all CNT loadings, including those of PLA alone, withstood compressive forces greater than typical skin insertion forces for microneedles (0.1–0.3 N)[35]. The PLA MNA's have previously been shown to penetrate mouse skin[21] and porcine skin (data not shown) with ease and thus served as a benchmark of mechanical strength for the composite MNA's in this study. Significant improvement in AFS were found between 3 wt% and 5 wt% ($p < 0.01$), between 4 wt% and 6 wt% ($p < 0.01$), and between 3 wt% and 6 wt% ($p < 0.0001$). The AFS was comparable to PLA microneedles at all CNT loadings tested, except at 3 wt%, where the AFS of the composite microneedles was significantly lower. These results indicate that intermolecular forces in the polymer may have been weakened by solvent casting. Hence, no further improvement was seen with the addition of *f*-MWCNT with respect to PLA. In comparison, the PLA MNA's were developed from non-solvent casted PLA, as these had been shown to penetrate the skin effectively.

In agreement with the literature, the SFS of composite microneedles were considerably lower than the AFS[36] (Figure 2B). This suggests that MNA's are more susceptible to failure from shear forces than axial forces[37]. Concerning the specific microneedle geometry, the SFS for the composite and PLA microneedles (>0.30 N) were moderately higher than that reported for MNA's made from another biodegradable polymer (PGA; 0.24 ± 0.05N) with a similar height and base diameter[36] (Figure 2B). For CNT loadings up to 5 wt%, the composite microneedles yielded significantly lower SFS in comparison to PLA ($p < 0.0001$). This further supports the notion that intermolecular forces in PLA were weakened by solvent casting the CNT-polymer composite. However, the SFS significantly improved at 6 wt% CNT loading in comparison to PLA. Taken together, the higher AFS and SFS at 6 wt% CNT loading were most probably a result of enhanced matrix stiffness and better interfacial interaction provided by the increased *f*-MWCNT loading, since the carboxyl groups can interact via hydrogen bonding with carbonyl groups in the PLA chains[38,39]. Therefore, MNA's made from 6 wt% CNT loading was utilised for the remainder of this study.

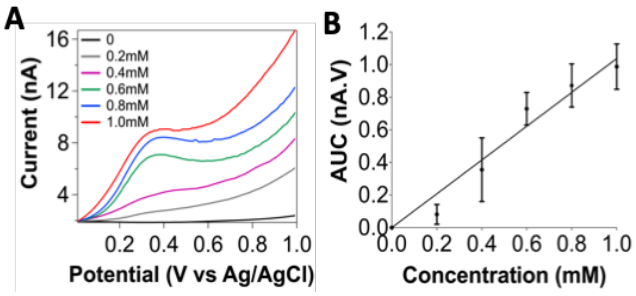

Figure 3. (A) Oxidative response of a single MNA towards different concentrations of AA measured by DPV (representative traces). (B) Calibration plot for the oxidative peak seen at 320 mV based on three MNA devices ($n = 3$).

Electrochemical characterisation. To demonstrate and evaluate the electrochemical performance of our MNA's, the oxidation of AA at the electrode surface was analysed using DPV. AA is an easily oxidisable, abundant antioxidant present in the skin with concentrations likely to be in the millimolar range[40]. Electrochemical determination of AA is challenging due its high overpotential for oxidation and fouling, induced by the adsorption of its oxidative product to electrode surfaces [41]. Here, the response towards AA was measured within 0.2–1 mM, and the representative DPV voltammograms are shown in Figure 3A. This shows an asymmetric anodic peak for all concentrations analysed, at a low potential of 0.320 ± 0.02 V. This is lower than measurements observed with a conventional unmodified platinum strip and carbon paste working electrode, where AA oxidative potentials were identified at 0.530 V and 0.470 V, respectively[42]. Hence, our results show the potential of CNT's to lower the overpotential required for AA oxidation and successfully alleviate the challenges above. Calibration data acquired by analysing the peak area for the oxidative responses at each concentration averaged from three MNA devices are shown in Figure 3B. This indicates a linear relationship between the concentration of AA and the current measured ($R^2 = 0.9282$). The limit of detection (LOD, determined as 3 times the standard deviation at the lowest concentration/slope of the calibration line) was 180 µM, with a signal-to-noise ratio at 4.8 and sensitivity at 1.113 nA·V mM^{-1}. A combination of low electroactive surface area and variation between electrodes, and the nature of them being composite electrodes, may explain the high LOD observed here. Nevertheless, the results show that our unmodified, non-conjugated polymeric nanocomposite MNA's are electroactive and possess good linearity over a wide detection range with detection limits that are fit for purpose for measurements in the skin.

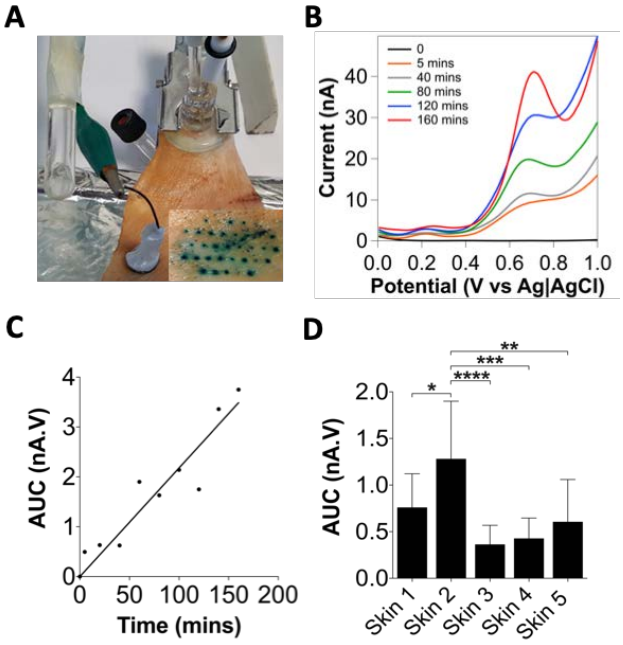

Figure 4. (A) Experimental set-up using a Franz diffusion cell for electrochemical measurements in the skin. *Inset* showing successful penetration of the microneedles visualised by methylene blue staining. (B) DPV traces after diffusion of PBS showing two distinct oxidative peaks within 5 minutes of PBS diffusion, at a potential of 0.3 V and 0.7 V. (C) Linear plot of AUC against time for the biggest change seen at 0.7 V. (D) Variation of the oxidative peak at 0.7 V across five skin samples (*$p < 0.05$, **$p < 0.01$, ***$p < 0.001$, ****$p < 0.0001$, one-way ANOVA with Tukey's multiple comparisons test, $n = 5$ animals).

***In situ* electrochemical performance in the skin.** *In situ* biosensing capabilities of the nanocomposite MNA was demonstrated by performing electrochemical measurements in freshly excised porcine ear skin. Figure 4A shows the experimental set-up implemented to allow diffusion of PBS through the skin. The skin was stretched to ensure successful penetration of all microneedles, as visualised by methylene blue staining (Figure 4A, inset). It was initially observed that, without diffusion, a small electrochemical response could not be detected from DPV measurements taken in the skin, regardless of time (Figure 4B, black line). Control measurement in the agarose gel also did not show an electrochemical response. In comparison to the skin, the baseline current was 10000-fold lower in the gel (see Supporting Information, Figure S1). After just 5 minutes of diffusion, two distinct oxidative peaks appeared, at 0.23 ± 0.02 V and 0.69 ± 0.04 V (Figure 4B). The precise nature of the electroactive species observed through this *in situ* measurement is unclear. The peaks may indicate the presence of dopamine and uric acid, which co-exist with AA at moderately high concentrations in the skin. Simultaneous detection of the aforementioned electroactive species remains an active area in biosensing research to date because their oxidative potentials overlap significantly, and detection of each analyte presents great clinical significance. In our research, it may be case that, the nanocomposite MNA's were detecting the abundantly present AA alongside either dopamine or uric acid. Other research has shown that CNT-modified electrodes are capable of detecting such electroactive species at non-overlapping potentials and can even do so simultaneously[43]. The peaks arose from the diffusion of electroactive species in the skin, to the electrode surface, as a result of the concentration gradient established by lateral diffusion of PBS. Therefore, the concentration should increase until an equilibrium had been established. The representative traces shown in Figure 4B does indicate a rise in concentration over time, but more prominently for the oxidative species at 0.69 V (by 634% after 160 minutes of PBS diffusion). Although the relationship seen here is linear (Figure 4C, $R^2 = 0.8939$), it may be assumed that an equilibrium would have been established over time. However, further resting DPV recordings were not taken beyond 160 minutes on this occasion. To ensure tissue integrity during the burn wound experiment, it was necessary to avoid prolonged incubation times that would lead to tissue deterioration. Nonetheless, since the magnitude of change was greater at 0.69 V, it was chosen for further analysis for the remainder of this study.

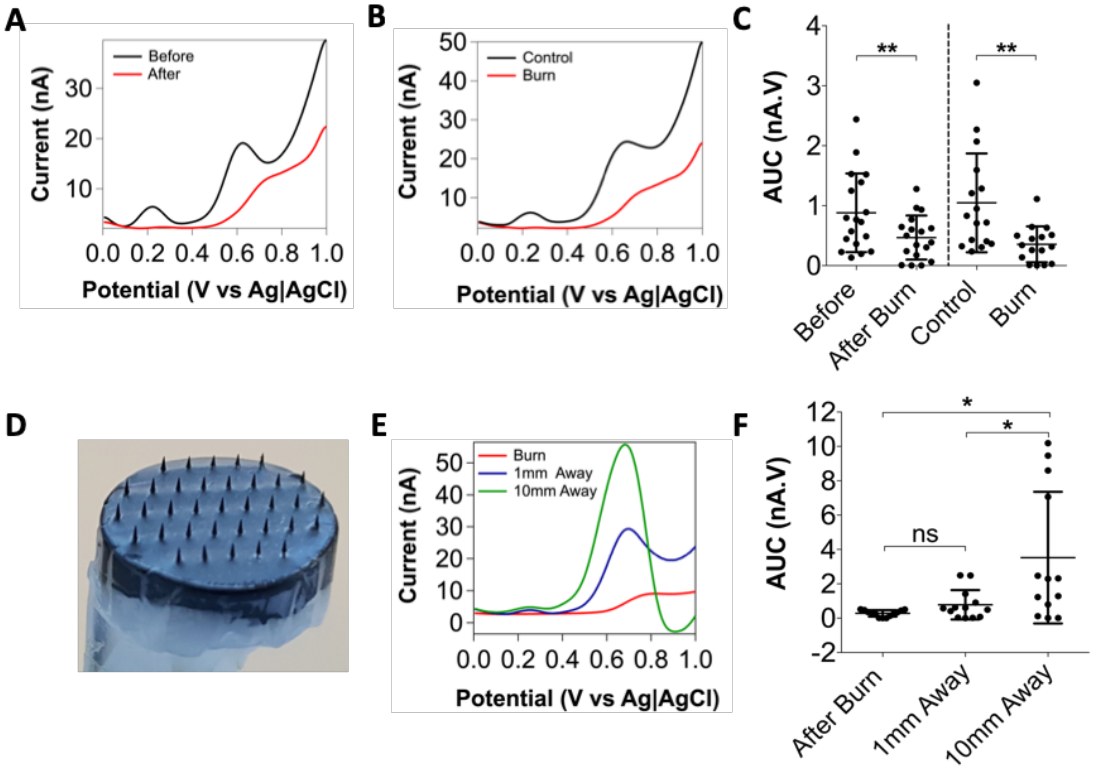

Figure 5. (A) Typical DPV responses before and after burn on the same skin area. (B) Typical DPV responses for a skin burn and an adjacent control (non-burn) skin area. Both traces show an attenuation of response for both oxidative peaks at 0.3 V and 0.7 V following the burn. (C) AUC of the oxidative peak at 0.7 V was significantly attenuated following thermal injury (**$p < 0.01$, two-tailed paired t-test). (D) Digital photograph of a MNA after 6 repeated skin insertions and removals, showing no evidence of mechanical failure. (E) Typical DPV responses obtained when measuring specific distances away from the burn site. (F) Differences in peak area at 0.7 V, measured at progressive distances away from the burn site. No significant difference was found between the burn site and 1 mm away, but significant differences exist between sites at 1 mm and 10 mm from the burn, as well as between the burn site and the 10 mm distant site (*$p < 0.05$, repeated measures one-way ANOVA with Tukey's test. Data are from 5 animals.

On repeating the DPV measurements across skin samples from five animals, a similar trend was found and importantly, both oxidative peaks were readily identifiable, earmarking this as a signature waveform. The variability among animals was assessed by measuring the oxidative response at 0.69 V after

160 minutes of PBS diffusion. This indicated a significant variation between animals (one-way ANOVA, $p = 0.001$) and the mean response was 0.687 ± 0.367 nA·V across all samples (Figure 4D). However, the variation was only statistically significant when comparing responses from all samples with that of skin 2, where the mean response was 1.282 ± 0.618 nA·V. The implication here is that, with the level of variation seen, we were unable to meaningfully assign a typical value for normal skin.

Burn wound model. The utility of the signature waveform as found here and hence the ability of our MNA's to monitor dynamic changes in the microenvironment of the skin was assessed by inducing artificial burn wounds. Two experimental conditions were investigated: (1) before and after burn measurements on the same skin site, and (2) comparing the burn site to an adjacent control (non-burn) site. Under both conditions, attenuation of the oxidative peak at 0.69 V was clear from the representative DPV traces shown in Figure 5A–B. This was found to be significant, as the oxidative response was suppressed by 0.4137 nA·V on the same skin site post-burn, and 0.6915 nA·V on the burn site compared to an adjacent control site ($p = 0.0070$ and $p = 0.0048$, respectively; two-tailed paired t-test, Figure 5C). This difference is unlikely to be due to diffusive or evaporative water loss caused by the application of heat, since this was accounted for by allowing PBS to re-diffuse into the burn site for 160 minutes. Neither is the difference likely to be due to the creation of microconduits in the skin by successive applications of MNAs because, in the second experimental condition, only the post-burn measurement was taken. The impact of any mechanical failure can also be excluded as there was no evidence of damage to the MNA after six repetitive insertions and removals (Figure 5D). A more likely explanation is that the biochemistry of the interstitium within the perimeters of the burn was altered due to the leakage of intracellular content from damaged cells. Furthermore, denaturing and cross-linking of proteins may also contribute to the attenuation of the response at 0.69 V. Nevertheless, our MNA's were able consistently measure the effect of thermal injury in the skin**.**

To determine whether the electrochemical waveform, as found here, would hold diagnostic value, we measured the impact of the burn on the skin at progressive distances away from the burn site. The representative DPV traces shown in Figure 5E indicates a trend where, consistent with the results described above, the oxidative response at 0.69 V was severely attenuated at the burn site (red line). Interestingly, the effect of the burn was still evident at a non-burn site located 1 mm from the burn site (blue line). However, measuring at a site 10 mm distant to the burn site revealed an oxidative response comparable to that of non-burn skin (black line). There was no significant difference between the burn and non-burn sites 1 mm away ($p = 0.0692$), whereas the non-burn sites located 10 mm away produced significantly higher responses ($p < 0.05$) compared to the burn site and the 1 mm non-burn site, with a mean difference of 3.245 nA·V and 2.746 nA·V, respectively (Figure 5F). This further confirms burn-induced suppression of the oxidative response at 0.69 V and, indicates that an equilibrium concentration for the oxidative species had not yet been established, despite the prolonged time allowed for PBS to diffuse through the skin. Collectively, these results show that the MNA-based sensors can distinguish between skin burns and normal (non-burn) skin. Thus, given further optimisation, our sensor may be of value in assessing the extent of a burn and monitoring burn wound recovery, by assessing the electrochemical changes in the skin.

CONCLUSIONS

We have fabricated solid MNA sensors from PLA/*f*-MWCNT composites by micromoulding. The fabrication steps discussed herein are simple and easy to scale up, with further adaptation possible using compression moulding or hot embossing technique allowing rapid manufacture. The nanocomposite MNA's have excellent mechanical properties for skin penetration and they were able to function well as *in situ* electrochemical biosensors. Our MNA sensors could rapidly monitor electrochemical changes in the skin, producing a signature waveform consisting of oxidative species that are yet to be identified. Characterisation of these species is currently underway as they may not only relate to skin pathologies as seen with the thermal injuries, but also can provide crucial information on electrochemical interferants for biosensing applications. Fabrication of only the working electrode is demonstrated here at present, but we envisage that reference and counter electrodes can be fabricated using a similar approach. MNA sensors produced from CNT-based composites can serve as a template for a range of sensors, due to the variety of modification strategies employable.

ASSOCIATED CONTENT

Supporting Information

Baseline current in non-skin control (PDF).

AUTHOR INFORMATION

Corresponding Author

*[1] E-mail: es415@brighton.ac.uk
*[1,3] E-mail: keng.ng@newcastle.ac.uk

Author Contributions

E.S., K.W.N., M.S.F. and B.A.P. designed the research. E.S. conducted the experiments and analysed the data. The manuscript was written by E.S. and revised by K.W.N., B.A.P., and M.S.F. All authors have given approval to the final version of the manuscript.

Notes

The authors declare no conflict of interest.

ACKNOWLEDGMENT

We thank Dr Ryan Waters (Pirbright Institute, Pirbright, UK) for donating the porcine ears used in this study. We are also grateful to Dr Andrew Flint and Dr Jonathan Salvage (Image Analysis Unit, University of Brighton) for their assistance with scanning electron microscopy.

REFERENCES

(1) Hosu, O.; Mirel, S.; Săndulescu, R.; Cristea, C. Minireview: Smart Tattoo, Microneedle, Point-Of-Care, and Phone-Based Biosensors for Medical Screening, Diagnosis, and Monitoring. *Anal. Lett.* **2017**, 1–15.

(2) Ventrelli, L.; Marsilio Strambini, L.; Barillaro, G. Microneedles for Transdermal Biosensing: Current Picture and Future Direction. *Adv. Healthc. Mater.* **2015**, *4* (17), 2606–2640.

(3) Windmiller, J. R.; Zhou, N.; Chuang, M.-C.; Valdés-Ramírez, G.; Santhosh, P.; Miller, P. R.; Narayan, R.; Wang, J. Microneedle Array-Based Carbon Paste Amperometric Sensors and Biosensors. *The Analyst* **2011**, *136* (9), 1846–1851.

(4) Miller, P. R.; Gittard, S. D.; Edwards, T. L.; Lopez, D. M.; Xiao, X.; Wheeler, D. R.; Monteiro-Riviere, N. A.; Brozik, S. M.; Pol-

sky, R.; Narayan, R. J. Integrated Carbon Fiber Electrodes within Hollow Polymer Microneedles for Transdermal Electrochemical Sensing. *Biomicrofluidics* **2011**, *5* (1), 013415.

(5) Mohan, A. M. V.; Windmiller, J. R.; Mishra, R. K.; Wang, J. Continuous Minimally-Invasive Alcohol Monitoring Using Microneedle Sensor Arrays. *Biosens. Bioelectron.* **2017**, *91*, 574–579.

(6) Mishra, R. K.; Vinu Mohan, A. M.; Soto, F.; Chrostowski, R.; Wang, J. A Microneedle Biosensor for Minimally-Invasive Transdermal Detection of Nerve Agents. *The Analyst* **2017**, *142* (6), 918–924.

(7) Miller, P. R.; Skoog, S. A.; Edwards, T. L.; Lopez, D. M.; Wheeler, D. R.; Arango, D. C.; Xiao, X.; Brozik, S. M.; Wang, J.; Polsky, R.; et al. Multiplexed Microneedle-Based Biosensor Array for Characterization of Metabolic Acidosis. *Talanta* **2012**, *88*, 739–742.

(8) Trzebinski, J.; Sharma, S.; Radomska-Botelho Moniz, A.; Michelakis, K.; Zhang, Y.; Cass, A. E. G. Microfluidic Device to Investigate Factors Affecting Performance in Biosensors Designed for Transdermal Applications. *Lab Chip* **2012**, *12* (2), 348–352.

(9) Moniz, A. R. B.; Michelakis, K.; Trzebinski, J.; Sharma, S.; Johnston, D. G.; Oliver, N.; Cass, A. Minimally Invasive Enzyme Microprobes: An Alternative Approach for Continuous Glucose Monitoring. *J. Diabetes Sci. Technol.* **2012**, *6* (2), 479–480.

(10) Skoog, S. A.; Miller, P. R.; Boehm, R. D.; Sumant, A. V.; Polsky, R.; Narayan, R. J. Nitrogen-Incorporated Ultrananocrystalline Diamond Microneedle Arrays for Electrochemical Biosensing. *Diam. Relat. Mater.* **2015**, *54*, 39–46.

(11) Keum, D. H.; Jung, H. S.; Wang, T.; Shin, M. H.; Kim, Y.-E.; Kim, K. H.; Ahn, G.-O.; Hahn, S. K. Microneedle Biosensor for Real-Time Electrical Detection of Nitric Oxide for In Situ Cancer Diagnosis During Endomicroscopy. *Adv. Healthc. Mater.* **2015**, *4* (8), 1153–1158.

(12) Yoon, Y.; Lee, G.; Yoo, K.; Lee, J.-B. Fabrication of a Microneedle/CNT Hierarchical Micro/Nano Surface Electrochemical Sensor and Its In-Vitro Glucose Sensing Characterization. *Sensors* **2013**, *13* (12), 16672–16681.

(13) Sharma, S.; Huang, Z.; Rogers, M.; Boutelle, M.; Cass, A. E. G. Evaluation of a Minimally Invasive Glucose Biosensor for Continuous Tissue Monitoring. *Anal. Bioanal. Chem.* **2016**, *408* (29), 8427–8435.

(14) Sharma, S.; Saeed, A.; Johnson, C.; Gadegaard, N.; Cass, A. E. Rapid, Low Cost Prototyping of Transdermal Devices for Personal Healthcare Monitoring. *Sens. Bio-Sens. Res.* **2017**, *13*, 104–108.

(15) McConville, A.; Davis, J. Transdermal Microneedle Sensor Arrays Based on Palladium: Polymer Composites. *Electrochem. Commun.* **2016**, *72*, 162–165.

(16) Spitalsky, Z.; Tasis, D.; Papagelis, K.; Galiotis, C. Carbon Nanotube–Polymer Composites: Chemistry, Processing, Mechanical and Electrical Properties. *Prog. Polym. Sci.* **2010**, *35* (3), 357–401.

(17) Yáñez-Sedeño, P.; Pingarrón, J. M.; Riu, J.; Rius, F. X. Electrochemical Sensing Based on Carbon Nanotubes. *TrAC Trends Anal. Chem.* **2010**, *29* (9), 939–953.

(18) Pumera, M.; Merkoçi, A.; Alegret, S. Carbon Nanotube-Epoxy Composites for Electrochemical Sensing. *Sens. Actuators B Chem.* **2006**, *113* (2), 617–622.

(19) Fagan-Murphy, A.; Patel, B. A. Compressed Multiwall Carbon Nanotube Composite Electrodes Provide Enhanced Electroanalytical Performance for Determination of Serotonin. *Electrochimica Acta* **2014**, *138*, 392–399.

(20) Fagan-Murphy, A.; Kataria, S.; Patel, B. A. Electrochemical Performance of Multi-Walled Carbon Nanotube Composite Electrodes Is Enhanced with Larger Diameters and Reduced Specific Surface Area. *J. Solid State Electrochem.* **2016**, *20* (3), 785–792.

(21) Ng, K. W.; Lau, W. M.; Williams, A. C. Towards Pain-Free Diagnosis of Skin Diseases through Multiplexed Microneedles: Biomarker Extraction and Detection Using a Highly Sensitive Blotting Method. *Drug Deliv. Transl. Res.* **2015**, *5* (4), 387–396.

(22) Gonçalves, C.; Gonçalves, I. C.; Magalhães, F. D.; Pinto, A. M. Poly(Lactic Acid) Composites Containing Carbon-Based Nanomaterials: A Review. *Polymers* **2017**, *9* (7), 269.

(23) Figueroa-Méndez, R.; Rivas-Arancibia, S. Vitamin C in Health and Disease: Its Role in the Metabolism of Cells and Redox State in the Brain. *Front. Physiol.* **2015**, *6*, 397.

(24) McAllister, D. V.; Wang, P. M.; Davis, S. P.; Park, J.-H.; Canatella, P. J.; Allen, M. G.; Prausnitz, M. R. Microfabricated Needles for Transdermal Delivery of Macromolecules and Nanoparticles: Fabrication Methods and Transport Studies. *Proc. Natl. Acad. Sci. U. S. A.* **2003**, *100* (24), 13755–13760.

(25) Lau, W. M.; Ng, K. W.; Sakenyte, K.; Heard, C. M. Distribution of Esterase Activity in Porcine Ear Skin, and the Effects of Freezing and Heat Separation. *Int. J. Pharm.* **2012**, *433* (1–2), 10–15.

(26) Liu, C.-X.; Choi, J.-W. Improved Dispersion of Carbon Nanotubes in Polymers at High Concentrations. *Nanomaterials* **2012**, *2* (4), 329–347.

(27) Gnanasekaran, K.; de With, G.; Friedrich, H. Quantitative Analysis of Connectivity and Conductivity in Mesoscale Multiwalled Carbon Nanotube Networks in Polymer Composites. *J. Phys. Chem. C* **2016**, *120* (48), 27618–27627.

(28) Bryning, M. B.; Islam, M. F.; Kikkawa, J. M.; Yodh, A. G. Very Low Conductivity Threshold in Bulk Isotropic Single-Walled Carbon Nanotube-Epoxy Composites. *Adv. Mater.* **2005**, *17* (9), 1186–1191.

(29) Aguilar, J. O.; Bautista-Quijano, J. R.; Aviles, F. Influence of Carbon Nanotube Clustering on the Electrical Conductivity of Polymer Composite Films. *Express Polym. Lett.* **2010**, *4* (5), 292–299.

(30) Mathur, R. B.; Pande, S.; Singh, B. P.; Dhami, T. L. Electrical and Mechanical Properties of Multi-Walled Carbon Nanotubes Reinforced PMMA and PS Composites. *Polym. Compos.* **2008**, *29* (7), 717–727.

(31) Ghislandi, M.; Tkalya, E.; Schillinger, S.; Koning, C. E.; de With, G. High Performance Graphene- and MWCNTs-Based PS/PPO Composites Obtained via Organic Solvent Dispersion. *Compos. Sci. Technol.* **2013**, *80*, 16–22.

(32) Atif, R.; Inam, F. Reasons and Remedies for the Agglomeration of Multilayered Graphene and Carbon Nanotubes in Polymers. *Beilstein J. Nanotechnol.* **2016**, *7*, 1174–1196.

(33) Atif, R.; Wei, J.; Shyha, I.; Inam, F. Use of Morphological Features of Carbonaceous Materials for Improved Mechanical Properties of Epoxy Nanocomposites. *RSC Adv* **2016**, *6* (2), 1351–1359.

(34) Bikiaris, D. Microstructure and Properties of Polypropylene/Carbon Nanotube Nanocomposites. *Materials* **2010**, *3* (4), 2884–2946.

(35) El-Laboudi, A.; Oliver, N. S.; Cass, A.; Johnston, D. Use of Microneedle Array Devices for Continuous Glucose Monitoring: A Review. *Diabetes Technol. Ther.* **2013**, *15* (1), 101–115.

(36) Park, J.-H.; Allen, M. G.; Prausnitz, M. R. Biodegradable Polymer Microneedles: Fabrication, Mechanics and Transdermal Drug Delivery. *J. Controlled Release* **2005**, *104* (1), 51–66.

(37) Khann, P.; Silv, H.; Bhansali, S. Variation in Microneedle Geometry to Increase Shear Strength. *Procedia Eng.* **2010**, *5*, 977–980.

(38) Wu, D.; Wu, L.; Zhang, M.; Zhao, Y. Viscoelasticity and Thermal Stability of Polylactide Composites with Various Functionalized Carbon Nanotubes. *Polym. Degrad. Stab.* **2008**, *93* (8), 1577–1584.

(39) Sobkowicz, M. J.; Sosa, R.; Dorgan, J. R. Supramolecular Bionanocomposites, Part 2: Effects of Carbon Nanoparticle Surface Functionality on Polylactide Crystallization. *J. Appl. Polym. Sci.* **2011**, *121* (4), 2029–2038.

(40) Juliet Pullar; Anitra Carr; Margreet Vissers. The Roles of Vitamin C in Skin Health. *Nutrients* **2017**, *9* (8), 866.

(41) Raj, C. R.; Ohsaka, T. Electroanalysis of Ascorbate and Dopamine at a Gold Electrode Modified with a Positively Charged Self-Assembled Monolayer. *J. Electroanal. Chem.* **2001**, *496* (1–2), 44–49.

(42) Pisoschi, A. M.; Pop, A.; Negulescu, G. P.; Pisoschi, A. Determination of Ascorbic Acid Content of Some Fruit Juices and Wine by Voltammetry Performed at Pt and Carbon Paste Electrodes. *Molecules* **2011**, *16* (2), 1349–1365.

(43) Pisoschi, A. M.; Pop, A.; Serban, A. I.; Fafaneata, C. Electrochemical Methods for Ascorbic Acid Determination. *Electrochimica Acta* **2014**, *121*, 443–460.

For TOC only

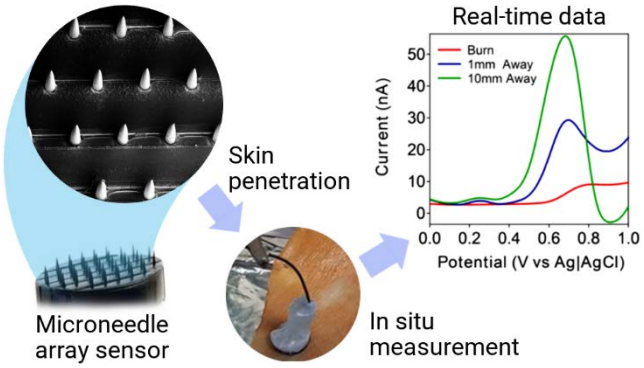
Real-time data
Burn
1mm Away
10mm Away
Current (nA)
50
40
30
20
10
0
0.0
0.2
0.4
0.6
0.8
1.0
Potential (V vs Ag|AgCl)
Skin
penetration
Microneedle
array sensor
In situ
measurement

Supporting information

Poly(lactic) acid/carbon nanotube composite microneedle arrays for dermal biosensing

Eldhose Skaria[*1], Bhavik A. Patel[1,2], Melanie S. Flint[1,2], Keng Wooi Ng[*1,3]

[1] School of Pharmacy and Biomolecular Sciences, University of Brighton, Huxley Building, Lewes Road, Brighton, BN2 4GJ, United Kingdom.
[2] Centre for Stress and Age-Related Diseases, University of Brighton, Huxley Building, Lewes Road, Brighton, BN2 4GJ, United Kingdom.
[3] School of Pharmacy, Faculty of Medical Sciences, Newcastle University, King George VI Building, Queen Victoria Road, Newcastle upon Tyne, NE1 7RU, United Kingdom.

* Corresponding authors: es415@brighton.ac.uk (E. Skaria); keng.ng@newcastle.ac.uk (K. W. Ng)

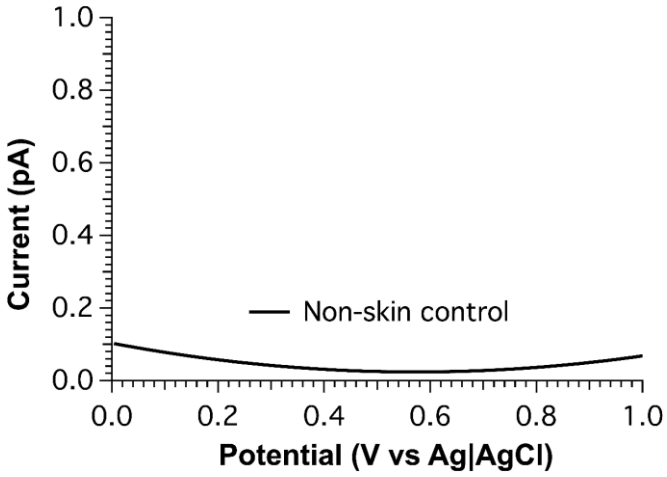

Figure S1: Baseline current in non-skin control (1% w/v agarose gel in 0.1 M phosphate buffered saline) measured by differential pulse voltammetry using the microneedle array sensor. Note that current on the vertical axis is expressed in picoamperes (pA). In skin experiments, the current was typically in the range of nanoamperes (nA).